

Cationic tantalum oxide nanoparticle contrast agent for micro computed tomography reveals articular cartilage proteoglycan distribution and collagen architecture alterations



Jiri Jäntti # † *, Anisha Joenathan ‡, Maria Fugazzola §, Juuso Tuppurainen # †, Juuso T.J. Honkanen ¶, Juha Töyräs † || ‡‡, René van Weeren §, Brian D. Snyder ##, Mark W. Grinstaff ‡ †‡, Hanna Matikka #, Janne T.A. Mäkelä # †

Diagnostic Imaging Center, Kuopio University Hospital, Kuopio, Finland

† Department of Technical Physics, University of Eastern Finland, Kuopio, Finland

‡ Division of Materials Science, Boston University, Boston, MA, USA

§ Department of Clinical Sciences, Utrecht University, Utrecht, The Netherlands

¶ Center of Oncology, Kuopio University Hospital, Kuopio, Finland

|| School of Electrical Engineering and Computer Science, The University of Queensland, Brisbane, Australia

Department of Orthopedic Surgery, Boston Children's Hospital, Boston, MA, USA

†† Departments of Biomedical Engineering and Chemistry, Boston University, Boston, MA, USA

‡‡ Science Service Center, Kuopio University Hospital, Kuopio, Finland

ARTICLE INFO

Article history:

Received 27 July 2023

Accepted 30 November 2023

Keywords:

Cartilage imaging

Micro computed tomography

Contrast agent

Nanoparticles

Diffusion

Osteoarthritis

SUMMARY

Objective: Cationic tantalum oxide nanoparticles (Ta_2O_5 -cNPs), as a newly introduced contrast agent for computed tomography of cartilage, offer quantitative evaluation of proteoglycan (PG) content and biomechanical properties. However, knowledge on the depth-wise impact of cartilage constituents on nanoparticle diffusion, particularly the influence of the collagen network, is lacking. In this study, we aim to establish the depth-dependent relationship between Ta_2O_5 -cNP diffusion and cartilage constituents (PG content, collagen content and network architecture).

Methods: Osteochondral samples ($n = 30$) were harvested from healthy equine stifle joints ($N = 15$) and the diffusion of 2.55 nm diameter cationic Ta_2O_5 -cNPs into the cartilage was followed with micro computed tomography (μCT) imaging for up to 96 hours. The diffusion-related parameters, Ta_2O_5 -cNP maximum partition (P_{max}) and diffusion time constant, were compared against biomechanical and depth-wise structural properties. Biomechanics were assessed using stress-relaxation and sinusoidal loading protocols, whereas PG content, collagen content and collagen network architecture were determined using digital densitometry, Fourier-transform infrared spectroscopy and polarized light microscopy, respectively.

Results: The P_{max} correlates with the depth-wise distribution of PGs (bulk Spearman's $\rho = 0.87$, $p < 0.001$). More open collagen network architecture at the superficial zone enhances intake of Ta_2O_5 -cNPs, but collagen content overall decreases the intake. The P_{max} values correlate with the equilibrium modulus ($\rho = 0.80$, $p < 0.001$) of articular cartilage.

Conclusion: This study establishes the feasibility of Ta_2O_5 -cNPs for the precise and comprehensive identification of biomechanical and structural changes in articular cartilage via contrast-enhanced μCT .

© 2023 The Author(s). Published by Elsevier Ltd on behalf of Osteoarthritis Research Society International.

This is an open access article under the CC BY license (<http://creativecommons.org/licenses/by/4.0/>).

Introduction

As the disease process of post-traumatic osteoarthritis (PTOA) progresses, the components of the articular cartilage, including proteoglycans (PGs) and collagen, degrade, and the collagen fibril network becomes disorganized. PGs create a negative fixed charge density in cartilage and are the main determinant of cartilage equilibrium stiffness.

* Correspondence to: Biophysics Group, Department of Technical Physics, Faculty of Science, Forestry and Technology, University of Eastern Finland, Yliopistonranta 8 F, 70210 Kuopio, Finland.

E-mail address: jiri.jantti@uef.fi (J. Jäntti).

<https://doi.org/10.1016/j.joca.2023.11.020>

1063-4584/© 2023 The Author(s). Published by Elsevier Ltd on behalf of Osteoarthritis Research Society International. This is an open access article under the CC BY license (<http://creativecommons.org/licenses/by/4.0/>).

On the other hand, the collagen network facilitates fluid pressurization within the cartilage upon instantaneous loading, thereby defining the instantaneous stiffness of cartilage. Degradation of these constituents increases permeability of articular cartilage, enables more unrestrained water flow out from the tissue during loading, and leads to significantly impaired load-bearing capacity of the articular cartilage.¹ Typically, microscopic deteriorations of cartilage remain hidden until the symptoms of PTOA occur (e.g., pain and difficulty in moving).² There is no cure for the disease. Fortunately, prompt identification of cartilage injuries following the joint trauma enables the implementation of pharmaceutical or surgical interventions that can prevent the progression of PTOA.^{3–5} Thus, diagnostic techniques to reveal early indicators of PTOA, e.g., microscopic deterioration of collagen network and PGs, are needed.

Current diagnostic techniques of PTOA, such as, magnetic resonance imaging (MRI), clinical examination, and native X-ray imaging are limited in their capability to detect acute cartilage injuries and initial changes in surrounding tissues. Modern computed tomography (CT) offers fast and high-resolution imaging with relatively good availability and low costs (e.g., compared to MRI). Furthermore, contrast-enhanced computed tomography (CECT) imaging allows visualization of soft tissues, such as cartilage when used together with radiopaque contrast agents. Conventional CT contrast agents for cartilage imaging are iodinated anionic or non-ionic molecules,^{6,7} however, pre-clinical cationic contrast agents, e.g., CA4+ (iodinated), possess advantages for cartilage imaging due to their ability to target the negatively charged PGs.^{7–11} This allows for direct and quantitative assessment of PG content¹² and, thus, cationic contrast agents can allow revealing early detection of PTOA. However, the impact of the collagen network organization on the diffusion of these molecules remains unclear. By comprehensively identifying the depth-dependent structural changes in cartilage constituents that substantially impact contrast agent diffusion, we can develop more effective contrast agents that accurately track the changes in key molecules, such as PGs and collagen, for improved disease diagnosis and monitoring.

Metallic nanoparticles (NPs) are an alternative contrast agent platform to small molecules, as their size, shape, and surface can be tailored.^{13,14} Tantalum and its oxides are biocompatible, chemically inert, and affordable materials,¹⁴ and are being investigated for different biomedical applications including coating of hip and knee joint replacements,¹⁵ implanted CT markers,¹⁶ and bone defect repair.^{17,18} Tantalum is also well-suited for CECT imaging due to its radiopacity and a specific energy point known as the *k*-edge at 67.4 keV.^{14,19} At this energy, tantalum exhibits a rapid increase in X-ray attenuation coefficient, resulting in improved contrast enhancement compared to conventional iodinated contrast agents. This enhanced contrast capability has been demonstrated in a swine obesity model,²⁰ highlighting the potential of tantalum agents in CECT imaging. Further, the size and surface of tantalum oxide NPs are easily modified e.g., to improve biocompatibility or targeting moieties of the NPs, and hence these NPs are applicable for multiple multimodal imaging and theranostic applications.^{21–23} Tantalum oxide NPs have been developed for CECT of vascular system,^{20,24,25} tumors,²⁵ and lymph nodes.²² With respect to cartilage imaging, Freedman et al.²¹ report the potential of tantalum oxide nanoparticles (Ta₂O₅-NPs) for visualization of cartilage, and Lawson et al.²⁶ describe Ta₂O₅-NPs for evaluating the glycosaminoglycan content and biomechanics of ex vivo human cadaveric metacarpal phalangeal joint cartilage.

In this study, we establish the depth-dependent cartilage structure-diffusion relationship of cationic tantalum oxide nanoparticles (Ta₂O₅-cNPs), assess their ability to distinguish two different load-bearing regions in cartilage, and evaluate their potential to reflect biomechanical properties of articular cartilage. We hypothesize that Ta₂O₅-cNPs will: 1) reveal the depth-wise PG distribution of articular cartilage in CECT; 2) diffuse into cartilage in a manner dependent on the collagen network due to the large size of the NP; and, 3) differentiate two load-bearing

areas and quantify the biomechanical properties. Experimentally, we harvested articular cartilage samples from healthy equines, conducted diffusion experiments of Ta₂O₅-cNPs using micro computed tomography (μ CT), employed comprehensive light microscopy and infrared spectroscopy to assess the cartilage structure, and conducted biomechanical testing to determine the functional properties of the cartilage.

Materials and methods

Samples

Cylindrical osteochondral samples ($d = 8.5$ mm), with non-degenerated cartilage, were extracted from stifle joints of healthy adult Criollo horses ($N = 15$, acquired from an abattoir) from two anatomical locations: distal intertrochlear groove ($n = 15$) and medial femoral condyle ($n = 15$). The samples were also utilized for another study.²⁷ The samples were stored in vials filled with isotonic phosphate-buffered saline (PBS) at -20 °C until the experiments.

Biomechanical testing

The cylindrical samples were thawed at room temperature and cartilage thickness was determined using μ CT (Nikon XT H 225 μ CT, Nikon Metrology Europe, Leuven, Belgium) by tomographic imaging of the samples in air (inside a sealed chamber to prevent drying). A four-step stress-relaxation²⁸ (a step size of 4% of remaining cartilage thickness, a ramp rate of 100%/s, 600 s relaxation between the steps), and a sinusoidal loading protocol²⁹ (4% peak-to-peak strain amplitude, 4 cycles, 1 Hz) were conducted in indentation geometry using a custom-made biomechanical testing device.²⁷ The biomechanical testing device consists of two main components: a displacement actuator with resolution of 0.1 μ m (PM1A11939, Newport, Irvine, CA, USA), and a load cell with resolution of 3.7 mN (Model 31, Honeywell International Inc., Charlotte, NC, USA). The osteochondral plugs were fixed at the bony end in a custom-made holder (three screws at the bottom, an acrylic edge, and a stainless-steel bed), which was filled with isotonic PBS (to allow comparing absolute moduli to previous experiments). A goniometer was used for positioning the cartilage surface perpendicular to the plane-ended cylindrical indenter ($d = 0.55$ mm). Full contact prior to the experiment was defined to be reached at 40 kPa pre-stress.

Dynamic modulus (E_{dyn}) and a phase shift (θ) were determined from the sinusoidal test.²⁹ The stress-relaxation protocol (excluding step 1) was used to determine Young's equilibrium modulus (E_{eq}), stress-relaxation time constant (α), and a stretching parameter (β).^{28,30} The time constant α reflects porosity, and an increase in α prolongs the time to reach relaxation equilibrium. The time constant β reflects the relaxation nonlinearity and is believed to be mainly driven by solid content, i.e., strained collagen fibers and PGs. In healthy tissue, β is high and relaxation is short and causes equilibrium to be attained at a higher load. Hayes correction was applied to account for the effect of indentation geometry on the results,³¹ and the Poisson's ratio was assumed to be 0.1 for the equilibrium and 0.5 (incompressible) for the dynamic modulus.^{32,33}

After biomechanical testing, the samples were halved for the histological sectioning and diffusion experiments. The half reserved for diffusion experiments was further divided into two quarters.

Contrast agent

The Ta₂O₅-cNPs were synthesized as previously described.²¹ The hydrodynamic diameter of Ta₂O₅-cNPs was 2.55 ± 0.96 nm as characterized by dynamic light scattering. The size of the particles was confirmed by transmission electron microscopy, and Fourier-transform infrared spectroscopy (FTIR) was used to verify amine conjugation on the particles (absorption band at 2919 cm^{-1}).

The contrast agent bath was prepared by dissolving the Ta₂O₅-cNPs (in powder) in PBS containing protease inhibitors ([5 mM, ethylenediamine-tetra-acetic acid disodium salt dihydrate (EDTA; VWR International, Radnor, PA, USA) and 5 mM benzamidine hydrochloride hydrate (Sigma-Aldrich Co., St. Louis, MO, USA)]. The pH was adjusted to 7.4 and osmolality to 400 mOsm/kg to correspond to the ionic strength of the synovial fluid.³⁴ The concentration of Ta₂O₅-cNPs was set to 30 mg/ml. To minimize the effect of dilution due to diffusion, the used contrast agent bath volume was 2.84 ml per sample, i.e., one hundred times the estimated cartilage volume.

Diffusion experiments and CECT imaging of cartilage

An overview of the diffusion experiments is presented in Fig. 1. The edges and the bottom of the osteochondral samples were sealed with cyanoacrylate (super glue, Loctite, Henkel AG, Düsseldorf, Germany) allowing diffusion of the Ta₂O₅-cNPs only through the articulating surface. The samples were immersed in the Ta₂O₅-cNP bath at 37 °C for 96 h, continuously shaken during immersion, and imaged in air with a Nikon XT H 225 µCT device (Nikon Metrology Europe, Leuven, Belgium) during the immersion period at different time points (0 h, 1 h, 2 h, 4 h, 6 h, 24 h, 48 h, 72 h, and 96 h). The images were acquired using 150 kVp tube voltage and 0.5 mm copper filtering. The samples were rotated full circle (360°) during the 6 min scan time while 1440 frames were imaged. The voxel size was 40 × 40 × 40 µm³.

Image analysis

Contrast agent partition profiles were established manually using a custom-made MATLAB (R2021b, MathWorks Inc., Natick, MA, USA) script as follows. The cartilage surface was rotated along x- and y-axis to achieve horizontal orientation of the sample surface. Air-cartilage and

cartilage-bone interfaces were detected based on X-ray attenuation thresholds from the middle of the sample. Using a region-of-interest (ROI) of 2.8 mm (diameter), depth-wise attenuation profiles were established by averaging the attenuation at each slice, and linearly interpolating to 100 points. The attenuation of native cartilage (0 h attenuation profile) was subtracted from each timepoint depth-dependently. Subsequently, the attenuation profiles were converted to partitions by dividing the depth-wise attenuation values by the attenuation of the contrast agent bath. Finally, diffusion curves were fitted to the time-dependent bulk partition data according to the equation:

$$P(t) = P_{\max} \times [1 - \exp(-t/\tau)], \quad (1)$$

where P_{\max} represents the partition at the equilibrium, t is the diffusion time, and τ is the diffusion time constant, i.e., the time required to reach 63.2% of the maximum partition.³⁵ Additionally, contrast agent partitions were computed separately for 5% depth-wise bins and the time-dependent partition equation was fitted to each bin independently.

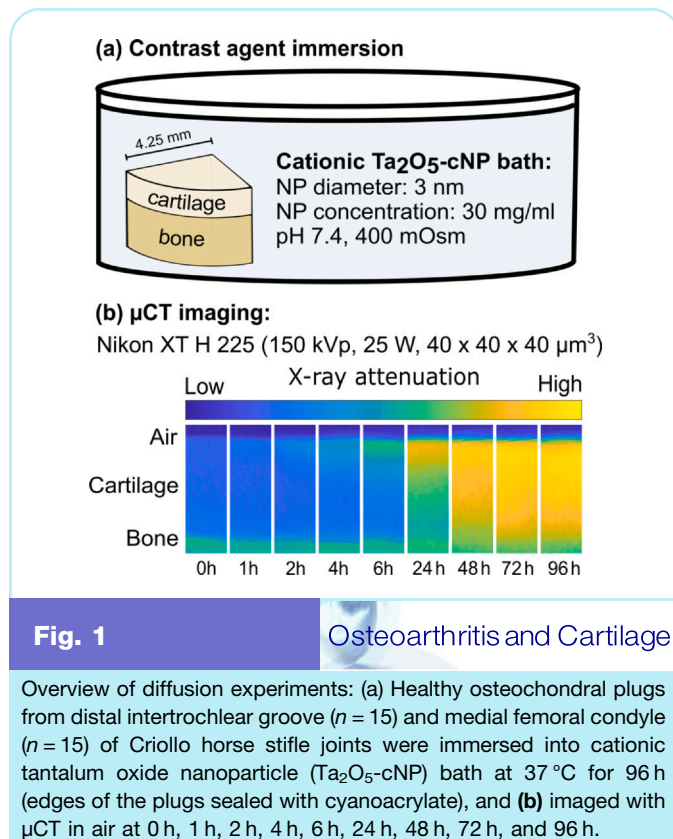
Microscopical and spectroscopical analysis

Digital densitometry, polarized light microscopy, and FTIR were used to map cartilage constituent contents and collagen network organization from histological sections. The halves that had not gone through the diffusion experiments were fixed in formalin for two weeks, decalcified in EDTA, dehydrated in graded alcohols, and embedded in paraffin as in previous studies.^{36,37} Next, 3 µm sections for digital densitometry, and 5 µm sections for FTIR and polarized light microscopy were sliced with a microtome perpendicularly to the cartilage surface. Digital densitometry sections were stained with 0.5% Safranin-O which binds stoichiometrically to negatively charged PGs revealing their location and quantity in direct proportion to the absorbance of light.^{38,39} These sections were additionally scored using the Mankin scoring system.⁴⁰

For digital densitometry, a light microscope (Nikon Microphot-FXA, Nikon Co., Tokyo, Japan), charge-coupled device camera (Hamamatsu ORCA-ER, Hamamatsu Photonics, Hamamatsu, Japan, pixel size = 3.09 µm × 3.09 µm), and a monochromator ($\lambda = 492 \pm 5$ nm) were used to capture grayscale images from the Safranin-O-stained sections. Grayscale images were converted to optical densities based on measured calibration filters (optical densities of 0.0, 0.15, 0.3, 0.6, 1.0, 1.3, 1.6, 2.0, 2.3, 2.6, and 3.0). Three sections of each sample were imaged. For each section, a depth-wise profile was generated by averaging pixels at the same depth. The average depth-wise profile of the samples was obtained by averaging their profiles from the three sections.^{38,41} The results are presented in a relative scale as experimental parameters for example, sample thickness and imaging setting, will affect the outcomes.

Collagen fiber network orientation and parallelism were measured using a polarized light microscopy system comprising a light microscope (Leitz Ortholux II POL, Leitz Wetzlar, Wetzlar, Germany) equipped with a monochromatic light source ($\lambda = 630 \pm 5$ nm, Edmund Optics Inc., Barrington, NJ, USA), two polarizers (Techspec optics® XP42–200, Edmund Optics, Barrington, NJ, USA), and a monochrome camera (BF-U3–88S6M-C FLIR Blackfly®, FLIR System Inc., Wilsonville, OR, USA, pixel size = 3.5 µm × 3.5 µm). Three sections of each sample were imaged. For each section, a depth-wise profile was generated by averaging pixels at the same depth. The average depth-wise profile of the samples was obtained by averaging their profiles from the sections.^{37,42}

Collagen content was determined using FTIR microscopy (Agilent Cary 670 spectrometer combined with Cary 620 infrared microscope, Agilent Technologies, Santa Clara, CA, USA, pixel size = 5.5 µm × 5.5 µm) by measuring the absorbance of the amide I region (1/



$\lambda = 1595\text{--}1720\text{ cm}^{-1}$),^{37,43} which has shown to directly correlate with collagen content.⁴⁴ One section of each sample was imaged and a depth-wise profile was generated by averaging pixels at the same depth. The results are presented in a relative scale as experimental parameters, for example, sample thickness and imaging setting, will affect the outcomes.

Before creating profiles for each section in the histological methods, the cartilage surface was orientated horizontally, and the ROI was cropped from the surface to the beginning of the cartilage-bone interface. Illustrative ROIs and depth-wise profiles of (a) PG content, (b) collagen content, (c) collagen orientation angle, and (d) collagen parallelism index, i.e., anisotropy (data published by Fugazzola²⁷) are presented in Fig. 2.

Statistical analyses

MATLAB was used for the statistical analyses. Means are presented with a corresponding 95% confidence interval (CI). Spearman correlation was used in evaluating the structure-diffusion and function-diffusion relationships. The limit for statistically significant differences was set to be $p < 0.05$. The correlations satisfying this criterion were described as strong ($|\rho| \geq 0.7$), moderate ($0.4 \leq |\rho| < 0.7$), or weak ($|\rho| < 0.4$). In addition, the Kruskal-Wallis test was used to study the statistical significance of differences in the diffusion characteristics (P_{\max} and τ) between cartilage extracted from the distal intertrochlear groove and medial femoral condyle. Two samples were excluded due to the inability to perform histological cutting, and one due to cracks on the articulating surface

originating from sample drilling (all three from medial femoral condyle), which led to the choice of performing the Kruskal-Wallis test instead of a paired test to keep all animals in the analysis.

Results

The uptake of 2.55 nm Ta₂O₅-cNPs into the medial femoral condyle was significantly greater compared to the distal intertrochlear groove at 6 h ($p = 0.017$) and at 24, 48, 72, and 96 h ($p < 0.001$). As depicted in Fig. 3a, the mean bulk P_{\max} value was 800% (95% CI 707, 893) and 372% (95% CI 282, 462) for the medial femoral condyle and distal intertrochlear groove, respectively, and differed significantly between the sites ($p < 0.001$). In both tissues, the τ increased as a function of depth (Fig. 3b). The mean bulk τ was 39 h (95% CI 17, 60) for the distal intertrochlear groove and 41 h (95% CI 24, 59) for the medial femoral condyle (Fig. 3b), which was not significantly different between the sites ($p = 0.20$).

Microscopy and spectroscopy results revealed that the samples from both locations were in good health, as indicated by the low Mankin scores (Table I). The P_{\max} value strongly positively correlated with PG content, moderately correlated with collagen orientation angle, and moderately inversely correlated with collagen content, parallelism index, and Mankin score as shown in Table I. The bulk τ moderately correlated with PG content, and moderately inversely correlated with collagen content and Mankin score (Table I).

When looking at the depth-wise P_{\max} profiles, they reflected the PG distribution in both locations (Fig. 4). The P_{\max} value had a

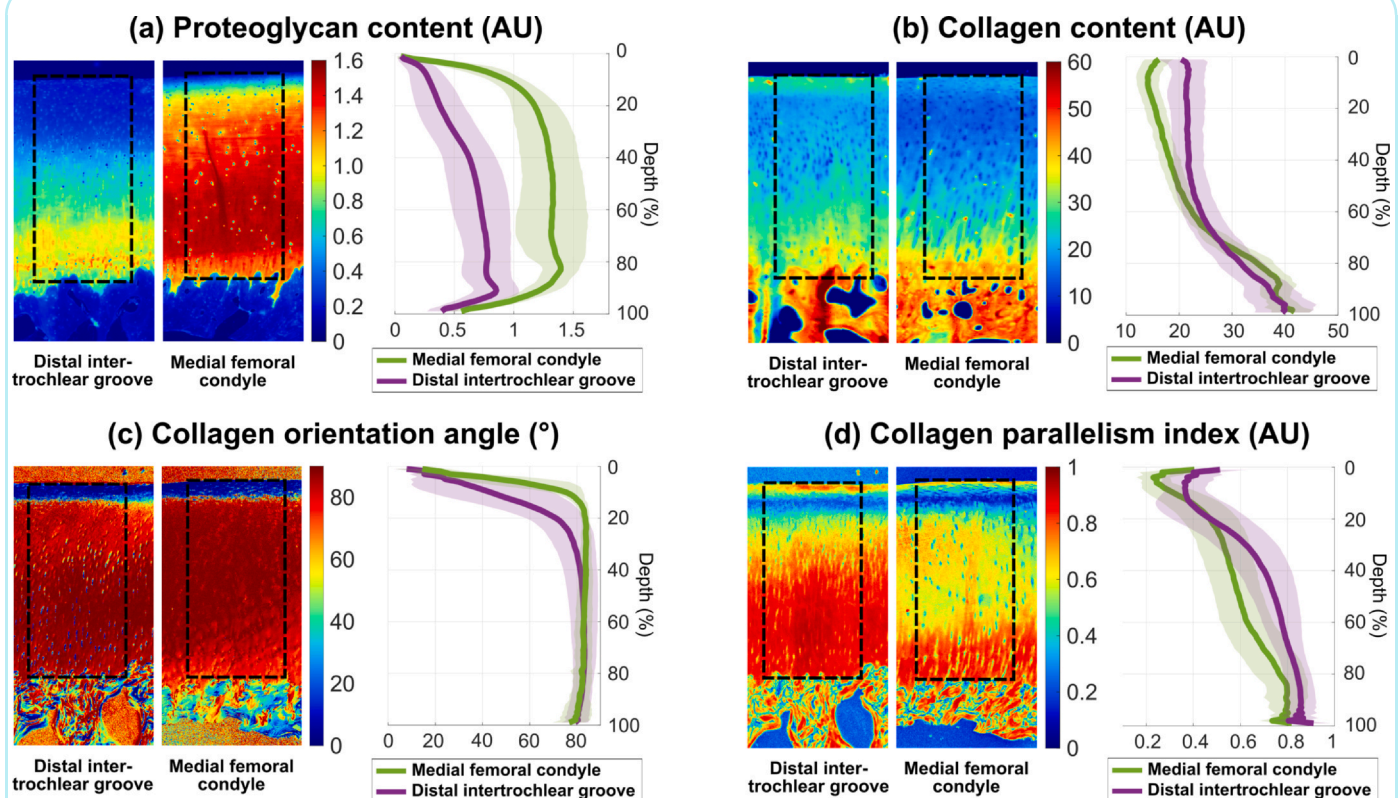


Fig. 2

Overview of cartilage structural and compositional properties: (a) PG content, (b) collagen content, (c) collagen orientation angle, and (d) collagen parallelism index. On the left, distributions of an example sample from the distal intertrochlear groove and medial femoral condyle are illustrated, and on the right, profiles of different histological properties (solid line) with standard deviation (shaded area) for 1% depth-wise bins are shown. 0% depth represents the articular surface and 100% the cartilage-bone interface. AU = arbitrary unit.

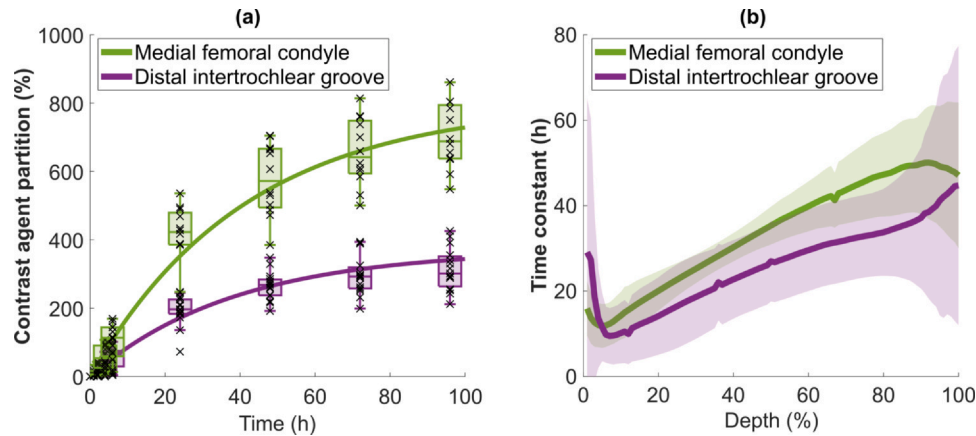


Fig. 3

Osteoarthritis and Cartilage

(a) Bulk Ta_2O_5 -cNP partition (tissue attenuation divided by contrast agent bath attenuation) in medial femoral condyle and distal intertrochlear groove as function of time. Data points are shown by x-markers. Box charts present means (solid horizontal line), upper (box above the mean) and lower (box below the mean) quantiles and the largest and smallest values (whiskers) at 1, 2, 4, 6, 12, 24, 48, 72, and 96 h for medial femoral condyle and distal intertrochlear groove. The exponential equation (Eq. 1) of medial femoral condyle ($\text{Partition}(t) = 800\% \times [1 - \exp(-t/41 \text{ h})]$) and distal intertrochlear groove ($\text{Partition}(t) = 372\% \times [1 - \exp(-t/39 \text{ h})]$). (b) Diffusion time constants (solid line) with standard deviation (shaded area) for 1% depth-wise bins of medial femoral condyle and distal intertrochlear groove ($n = 23$, four samples were excluded from the illustration based on Grubbs outlier test).

significant depth-wise relationship with all the structural parameters (Fig. 5a). In a depth-wise manner, τ positively correlated with PG content (Fig. 5b). The relationship between the Ta_2O_5 -cNP partition and the cartilage structure properties also varied over time (Fig. 6). Initially, correlations were observed in the superficial zone, which with longer diffusion times progressed to the deep zone eventually, as depicted in Fig. 6.

The P_{\max} value strongly correlated with biomechanics (Table II): correlation was strong with E_{eq} and β ; moderate with α and E_{dyn} . A

strong inverse correlation was found between the P_{\max} and phase shift θ . Moreover, τ moderately correlated with E_{eq} and E_{dyn} , as shown in Table II.

Discussion

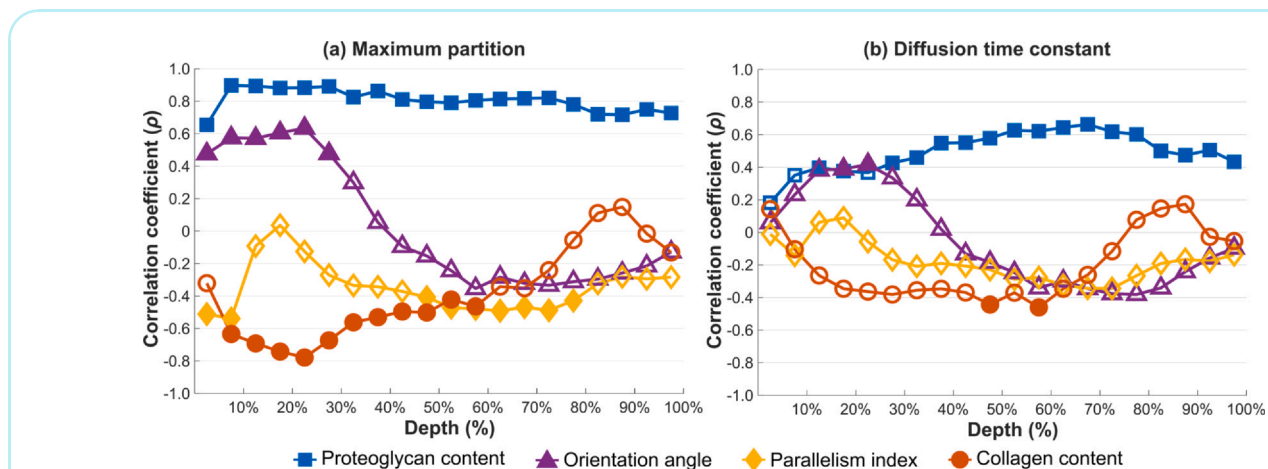
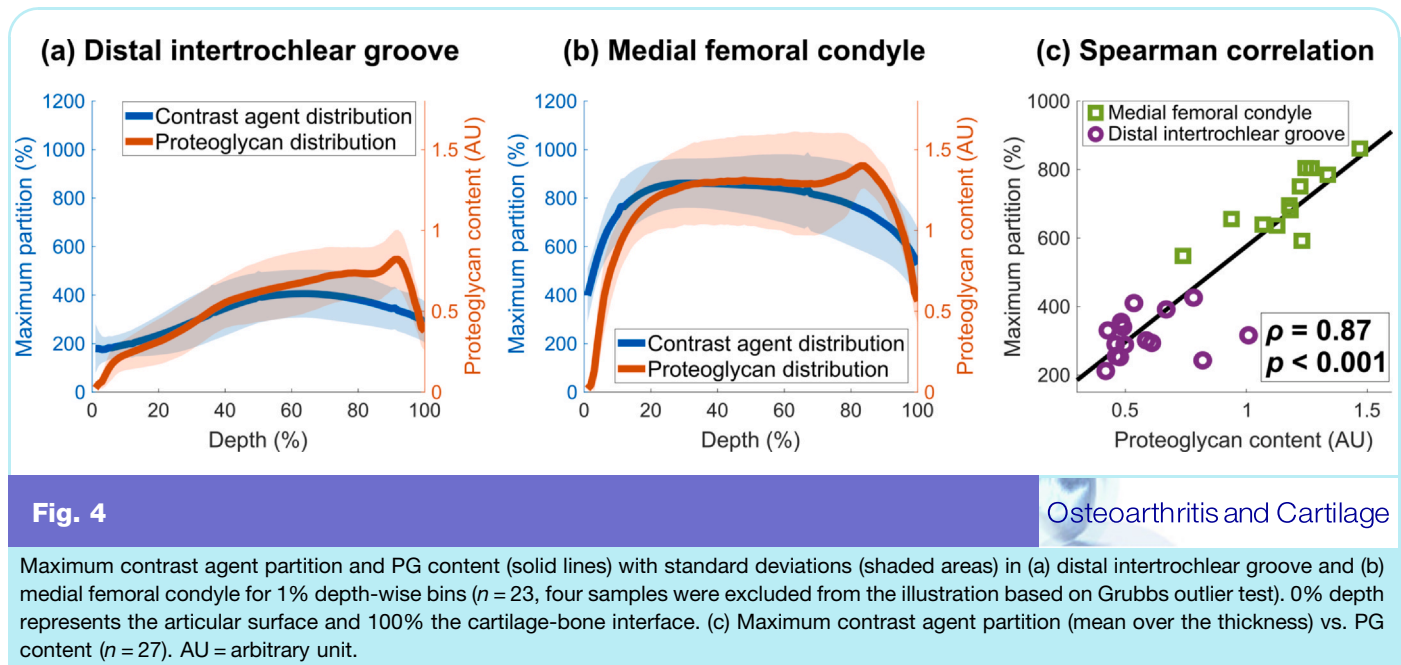
We investigated the impact of depth-dependent variations in articular cartilage composition on the diffusion of Ta_2O_5 -cNPs by CECT. Using osteochondral samples harvested from healthy equine

(a) Spearman correlation coefficient, ρ (95% confidence interval)					
	PG content	Collagen content	Parallelism index	Orientation angle	Mankin score
Maximum partition, P_{\max}	0.87 (0.73, 0.94) $p < 0.001$	-0.55 (-0.77, -0.22) $p = 0.003$	-0.45 (-0.71, -0.08) $p = 0.020$	0.47 (0.11, 0.72) $p = 0.014$	-0.52 (-0.75, -0.17) $p = 0.005$
Diffusion time constant, τ	0.46 (0.09, 0.71) $p = 0.017$	-0.42 (-0.69, -0.05) $p = 0.027$	-0.12 (-0.48, 0.27) $p = 0.56$	0.19 (-0.21, 0.53) $p = 0.34$	-0.42 (-0.69, -0.05) $p = 0.028$
(b) Average \pm standard deviation (95% confidence interval)					
	PG content (AU)	Collagen content (AU)	Parallelism index (AU)	Orientation angle ($^\circ$)	Mankin score
Distal intertrochlear groove	0.58 ± 0.17 (0.49, 0.68)	25.79 ± 2.97 (24.15, 27.43)	0.68 ± 0.09 (0.63, 0.73)	16.52 ± 6.46 (12.94, 20.10)	1.74 ± 0.80 (1.30, 2.19)
Medial femoral condyle	1.17 ± 0.19 (1.05, 1.28)	23.42 ± 1.59 (22.44, 24.40)	0.59 ± 0.10 (0.53, 0.65)	11.11 ± 3.34 (9.04, 13.18)	0.87 ± 0.51 (0.55, 1.29)

Table I

Osteoarthritis and Cartilage

(a) Spearman correlation coefficient (ρ) between bulk contrast agent diffusion characteristics (P_{\max} and τ) and structural properties: PG content, collagen content, parallelism index, and orientation angle, defined from full thickness of cartilage, and Mankin score. Statistical significance ($p < 0.05$) is indicated by bold. (b) The average values of the measured structural properties. AU = arbitrary unit.



stifle joints, exhibiting varied mechanical properties and structure characteristics, we determined P_{\max} and τ as a function of cartilage depth. Prior studies reported the relationship between cartilage structure and contrast agent diffusion to overall or large sectional analyses.^{21,26,45–47} To our knowledge, this is the first time that the depth-dependent effect of articular cartilage structure on NP contrast agent diffusion has been explored incrementally (in 5% windows) over the full cartilage thickness.

A strong positive correlation exists between P_{\max} and PG content ($\rho = 0.87$, $p < 0.001$; Table I and Fig. 4c). This correlation is consistent with previous findings reported for cationic contrast agents,^{21,26,30,45} and in agreement with Lawson et al. who also

utilized cationic Ta₂O₅-NPs.²⁸ μ CECT imaging is capable of distinguishing between samples harvested from different locations within the joint (Fig. 3a). Importantly, Ta₂O₅-cNP contrast agent distribution reflects PG distribution throughout the cartilage thickness (Figs. 4a and b), offering a method for 3D determination of PG content without the need for conventional sample preparation or cutting of the sections. A correlation was observed between the partition of Ta₂O₅-cNP and PG content in the superficial zone at the 6-hour time point (Fig. 6a), as well as in all cartilage zones after 48 hours. The diffusion of Ta₂O₅-cNPs into the cartilage was found to persist for up to 96 hours of immersion. To expedite the process of 3D histology, accurate assessment of PG distribution before reaching diffusion

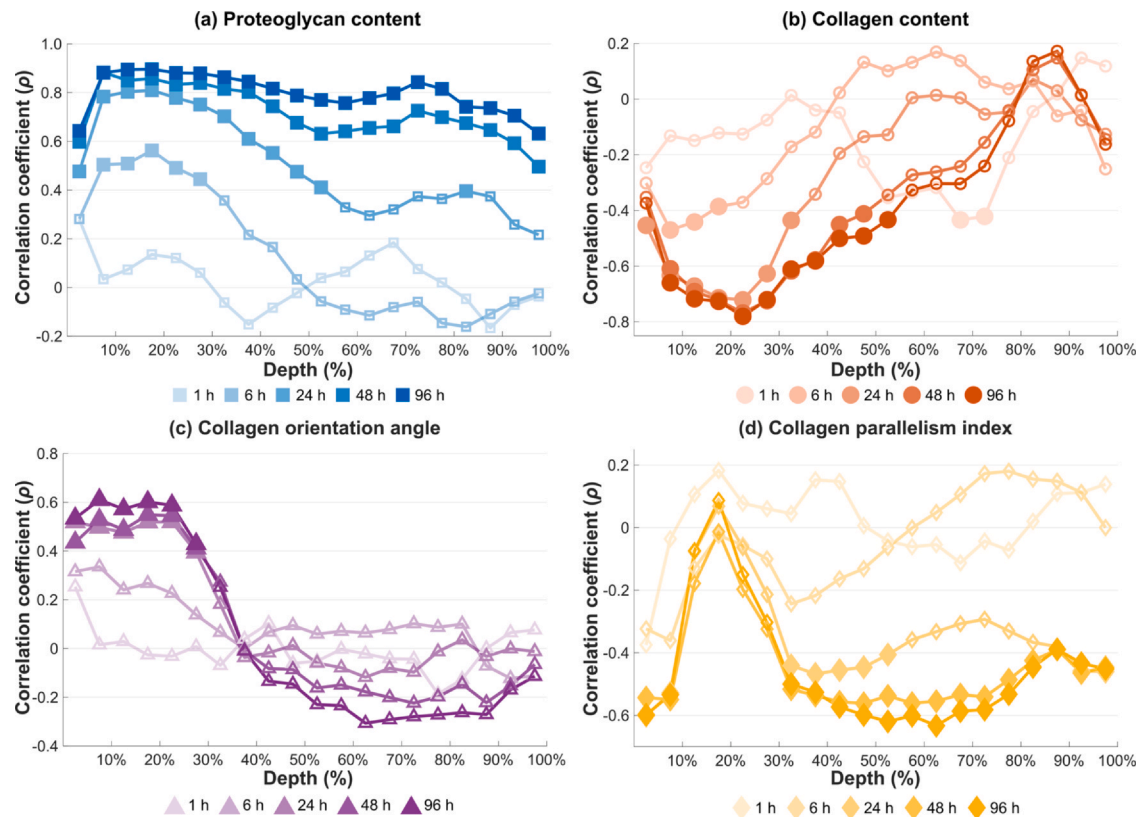


Fig. 6

Osteoarthritis and Cartilage

Time-dependent effect on depth-wise Spearman correlation coefficient between Ta_2O_5 -cNP partition and (a) PG content, (b) collagen content, (c) collagen orientation angle, (d) collagen parallelism index, determined from 5% windows, at 1 h, 6 h, 24 h, 48 h, and 96 h. 0% depth represents the articular surface and 100% the cartilage-bone interface. A filled marker indicates a statistically significant ($p < 0.05$) correlation and an open marker not significant ($p > 0.05$) correlation.

equilibrium is feasible but may require multiple measurements. Alternatively, allowing the contrast agent to diffuse through all sides of the samples can be employed.


The current results demonstrate a significant correlation between the large Ta_2O_5 -cNP contrast agent intake and collagen characteristics, including collagen content, orientation angle, and parallelism index (Table 1 and Fig. 5). Previously, the cationic iodinated contrast agent CA4+, has weakly correlated with the collagen content ($\rho = 0.171$, $p = 0.05$),³⁰ which disagrees with our finding ($\rho = -0.55$, $p = 0.003$), and is likely an indirect result of correlation between collagen and PG content (that binds CA4+). It is worth noting that Ta_2O_5 -cNPs (diameter = 2.55 nm) are twice as large as CA4+,¹¹ enabling them to reflect collagen characteristics more effectively. Consequently, the diffusion of Ta_2O_5 -cNPs is inversely related to collagen content, a factor known to modulate cartilage permeability.⁴⁸ In the depth-wise analysis, we observed that an increased collagen orientation angle in the superficial and mid zones, indicative of a more open collagen network architecture, enhances P_{max} . Similarly, a higher anisotropy in the superficial and deep zones also contributes to this effect.

To the best of our knowledge, this study represents the first investigation into the correlation between the diffusion time τ and cartilage structure, although τ for CA4+ is known to differ between different cartilage types⁴⁹ and regions within the joint (e.g., medial vs. lateral femoral condyles).¹² Boos et al.⁴⁹ report the largest τ value in cartilage tissue with the greatest PG content when using cationic

CA4+, which is consistent with the present findings. Conversely, higher collagen content decreases τ as it increases steric hindrance and reduces fluid flow in articular cartilage.⁵⁰ This observation has not been previously reported for molecule-based contrast agents, supporting our hypothesis that larger NPs may be more influenced by the collagen matrix.

Depth-wise analysis of the τ reveals a linear increase relative to depth (Fig. 3b), with τ being 2.6 times slower at 50% depth and 3.7 times slower at 80% depth compared to 20% depth. The finding agrees with that reported by Honkanen et al.⁵¹ who show accumulation of the cationic contrast agent (CA2+) into the deep zone prolonging diffusion. The mean τ , depends on the total amount of NPs diffusing into the tissues, which increases with higher PG content (Table 1). Similarly, diffusion equilibrium is reached later in samples with smaller Mankin score (i.e., healthier tissue) which is seen as an inverse correlation between τ and the Mankin score ($\rho = -0.42$, $p = 0.028$). While waiting for Ta_2O_5 -cNP diffusion to reach bulk equilibrium throughout the cartilage may not be clinically feasible, however, modern clinical CTs have sufficient resolution to examine the cartilage superficial zone where equilibrium or sufficient partition for the assessment of PG content and collagen characteristics is reached earlier (average minimum for both locations $\tau = 16.2$ (95% CI 9.4, 23.0), Fig. 3b). It is noteworthy that a correlation between Ta_2O_5 -cNP partition and superficial PGs, as well as collagen content, became observable after six hours (Fig. 6). This observation

(a) Spearman correlation coefficient, ρ (95% confidence interval)					
	E_{eq}	α	β	E_{dyn}	θ
Maximum partition, P_{max}	0.80 (0.60, 0.90) $p < 0.001$	0.67 (0.39, 0.84) $p < 0.001$	0.71 (0.45, 0.86) $p < 0.001$	0.46 (0.10, 0.72) $p = 0.016$	-0.73 (-0.87, -0.48) $p < 0.001$
Diffusion time constant, τ	0.41 (0.03, 0.68) $p = 0.034$	0.29 (-0.10, 0.61) $p = 0.14$	0.24 (-0.16, 0.57) $p = 0.24$	0.51 (0.16, 0.75) $p = 0.006$	-0.34 (-0.64, 0.05) $p = 0.09$
(b) Average \pm standard deviation (95% confidence interval)					
	E_{eq} (MPa)	α (s)	β	E_{dyn} (MPa)	θ (°)
Distal intertrochlear groove	0.55 \pm 0.26 (0.41, 0.70)	5.71 \pm 2.72 (4.21, 7.22)	0.39 \pm 0.03 (0.37, 0.41)	4.88 \pm 0.86 (4.40, 5.35)	16.28 \pm 3.20 (14.51, 18.05)
Medial femoral condyle	1.42 \pm 0.54 (1.08, 1.75)	11.74 \pm 4.83 (8.75, 14.73)	0.50 \pm 0.05 (0.47, 0.53)	6.13 \pm 2.67 (4.48, 7.78)	10.31 \pm 3.70 (8.02, 12.59)

Table II  Osteoarthritis and Cartilage

(a) Spearman correlation coefficient between bulk diffusion characteristics (P_{max} and τ) and the biomechanical properties: equilibrium modulus (E_{eq}), stress-relaxation time constant (α), stretching parameter (β), dynamic modulus (E_{dyn}), and phase shift (θ) for distal intertrochlear groove and medial femoral condyle. E_{eq} , α , and β are derived analytically from the stress-relaxation test, and E_{dyn} , and θ are derived analytically from the sinusoidal dynamic test. Statistical significance ($p < 0.05$) is indicated by bold typeface. (b) The average values of the measured biomechanical properties.

is significant because the superficial zone, where osteoarthritis (OA) and associated cartilage degeneration often initiate, had sufficient contrast agent presence to reveal the correlation.^{37,43,52–54}

The correlation between P_{max} and equilibrium modulus, E_{eq} , is strong as expected (Table II): PGs contribute to the equilibrium stiffness of articular cartilage and cationic NPs are attracted to them. The P_{max} correlates with the stress-relaxation time constant, α , and the stretching parameter, β . This result agrees with a previous study investigating cationic contrast agent (CA4+)³⁰ which reported lower α and β values in samples from defect areas compared to healthy control samples. The ability of Ta₂O₅-cNPs to reflect E_{eq} of articular cartilage shows their potential to reveal possible impairment in articular cartilage load-bearing capability,^{36,37} whereas α and β , reflect changes in tissue permeability.³⁰ The phase shift θ , correlates inversely with P_{max} , indicating more Ta₂O₅-cNPs diffusing into healthier and more elastic tissue, whereas E_{dyn} positively correlates with τ , indicating that diffusion equilibrium is reached later in samples with a greater dynamic modulus, which is influenced by collagen.³⁷

The present results do not provide insight into the capability of Ta₂O₅-cNPs to detect PTOA changes in cartilage as the samples studied were healthy. These findings in healthy cartilage establish a crucial foundation for subsequent investigations aiming at assessing the diagnostic potential and discriminative power of the agent to detect and potentially grade OA lesions. However, the variation of structural and biomechanical properties in the present samples is consistent with changes observed in the early onset of the disease.^{37,55} Future studies will expand the scope to investigate PTOA models based on the universal structure-diffusion relationship established in this study. We conducted our study using Ta₂O₅-cNPs that were specifically designed to penetrate healthy equine cartilage, and we did not explore different NP compositions. Nonetheless, the size of the present NPs was limited by the pore size of human cartilage, which is less than 6 nm.⁵⁶ For other applications, a range of nanomaterials with various particle sizes could be considered.^{57–59} Also, the material of the contrast agent for CT imaging needs to be highly attenuating to achieve good contrast. As photon-counting detector CT technology becomes more widely available, there is a growing interest in using high k -edge elements like tantalum for contrast imaging.¹⁴ The large difference in k -edge between two or more

contrast agents allows dual- or even multi-contrast-enhanced CT imaging of cartilage,^{9,10,47} which makes tantalum to be desirable candidate for spectral imaging combined with an iodinated contrast agent.

In summary, we report the feasibility of using Ta₂O₅-cNPs as a contrast agent for articular cartilage imaging. Contrast-enhanced μ CT with Ta₂O₅-cNPs detects differences in various parameters of cartilage constituents in a depth-dependent manner, including PG content and the collagen fibril network. Ta₂O₅-cNP maximum partition, P_{max} , strongly and positively correlates with the PG content and equilibrium modulus, and moderately with collagen orientation angle. It moderately inversely correlates with collagen content, parallelism index, and Mankin score. In a depth-wise manner, P_{max} positively correlates with PG content and collagen orientation angle, and inversely with collagen content and parallelism index. Overall, CECT using the Ta₂O₅-cNP contrast agent is most sensitive to the changes in structure and biomechanical properties of the cartilage superficial zone. Ta₂O₅-cNPs are a novel type of contrast agent for articular cartilage imaging and for quantitative assessment of pivotal markers associated with cartilage health: PG content, collagen architecture, and biomechanical performance.

Role of the funding sources

The funders were not involved in study design, data collection, data analysis, data interpretation, writing of the manuscript, or decision to publish.

Declaration of Competing Interest

The authors have no competing interests to declare regarding this manuscript.

Declaration of generative AI and AI-assisted technologies in the writing process

During the preparation of this work, the author(s) used ChatGPT-3.5 to improve the readability and language of the manuscript. After using

this tool, the author(s) reviewed and edited the content as needed and take(s) full responsibility for the content of the publication.

Acknowledgments

Instrumentarium Science Foundation (220009, 190021), Finnish Cultural Foundation – Central Fund (00220411), Alfred Kordelin Foundation (220016), Orion Research Foundation sr, Competitive State Research Funding of the Kuopio University Hospital Catchment Area (5063579, 5041810), Academy of Finland (307932, 348410, 357787), Regional Council of Pohjois-Savo (A74798), and Biocenter Kuopio are acknowledged for financial and infrastructural support. Eija Rahunen is acknowledged for the preparation of histological sections, Mikko Nissinen for sample preparation, planning of biomechanical testing and scoring of histological samples, and Santtu Mikkonen for his expertise in statistics.

Author contributions

Conception and design: All authors.

Collection, assembly, and analysis of data: Jiri Jäntti, Anisha Joenathan, Maria Fugazzola, Juuso Tuppurainen.

Drafting of the article: Jiri Jäntti.

Revising the article critically for important intellectual content: All authors.

Final approval of the article: All authors.

References

- Setton LA, Elliott DM, Mow VC. Altered mechanics of cartilage with osteoarthritis: human osteoarthritis and an experimental model of joint degeneration. *Osteoarthritis Cartil* 1999;7(1):2–14. <https://doi.org/10.1053/joca.1998.0170>
- Punzi L, Galozzi P, Luisetto R, Favero M, Ramonda R, Oliviero F, et al. Post-traumatic arthritis: overview on pathogenic mechanisms and role of inflammation. *RMD Open* 2016;2(2), e000279. <https://doi.org/10.1136/rmdopen-2016-000279>
- Bay-Jensen AC, Hoegh-Madsen S, Dam E, Henriksen K, Sondergaard BC, Pastoureau P, et al. Which elements are involved in reversible and irreversible cartilage degradation in osteoarthritis? *Rheumatol Int* 2010;30(4):435–42. <https://doi.org/10.1007/s00296-009-1183-1>
- Anderson DD, Chubinskaya S, Guilak F, Martin JA, Oegema TR, Olson SA, et al. Post-traumatic osteoarthritis: Improved understanding and opportunities for early intervention. *J Orthop Res* 2011;29(6):802–9. <https://doi.org/10.1002/jor.21359>
- Olson SA, Furman BD, Kraus VB, Huebner JL, Guilak F. Therapeutic opportunities to prevent post-traumatic arthritis: Lessons from the natural history of arthritis after articular fracture. *J Orthop Res* 2015;33(9):1266–77. <https://doi.org/10.1002/jor.22940>
- Kokkonen HT, Suomalainen JS, Joukainen A, Kröger H, Sirola J, Jurvelin JS, et al. In vivo diagnostics of human knee cartilage lesions using delayed CBCT arthrography. *J Orthop Res* 2014;32(3):403–12. <https://doi.org/10.1002/jor.22521>
- Lusic H, Grinstaff MW. X-ray-computed tomography contrast agents. *Chem Rev* 2013;113(3):1641–66. <https://doi.org/10.1021/cr200358s>
- Stewart RC, Patwa AN, Lusic H, Freedman JD, Wathier M, Snyder BD, et al. Synthesis and preclinical characterization of a cationic iodinated imaging contrast agent (CA4+) and its use for quantitative computed tomography of ex vivo human hip cartilage. *J Med Chem* 2017;60(13):5543–55. <https://doi.org/10.1021/acs.jmedchem.7b00234>
- Bhattarai A, Honkanen JTJ, Myller KAH, Prakash M, Korhonen M, Saukko AEA, et al. Quantitative dual contrast CT technique for evaluation of articular cartilage properties. *Ann Biomed Eng* 2018;46(7):1038–46. <https://doi.org/10.1007/s10439-018-2013-y>
- Honkanen MKM, Saukko AEA, Turunen MJ, Xu W, Lovric G, Honkanen JTJ, et al. Triple contrast CT method enables simultaneous evaluation of articular cartilage composition and segmentation. *Ann Biomed Eng* 2020;48(2):556–67. <https://doi.org/10.1007/s10439-019-02362-6>
- Bansal PN, Stewart RC, Entezari V, Snyder BD, Grinstaff MW. Contrast agent electrostatic attraction rather than repulsion to glycosaminoglycans affords a greater contrast uptake ratio and improved quantitative CT imaging in cartilage. *Osteoarthritis Cartil* 2011;19(8):970–6. <https://doi.org/10.1016/j.joca.2011.04.004>
- Nelson BB, Stewart RC, Kawcak CE, Freedman JD, Patwa AN, Snyder BD, et al. Quantitative evaluation of equine articular cartilage using cationic contrast-enhanced computed tomography. *Cartilage* 2021;12(2):211–21. <https://doi.org/10.1177/1947603518812562>
- Liu Y, Ai K, Lu L. Nanoparticulate X-ray computed tomography contrast agents: from design validation to in vivo applications. *Acc Chem Res* 2012;45(10):1817–27. <https://doi.org/10.1021/ar300150c>
- Yeh BM, FitzGerald PF, Edic PM, Lambert JW, Colborn RE, Marino ME, et al. Opportunities for new CT contrast agents to maximize the diagnostic potential of emerging spectral CT technologies. *Adv Drug Delivery Rev* 2017;113:201–22. <https://doi.org/10.1016/j.addr.2016.09.001>
- Balagna C, Faga MG, Spriano S. Tantalum-based multilayer coating on cobalt alloys in total hip and knee replacement. *Mater Sci Eng: C* 2012;32(4):887–95. <https://doi.org/10.1016/j.msec.2012.02.007>
- Olivecrona H, Maguire GQ, Noz ME, Zeleznik MP, Kesteris U, Weidenhielm L. A CT method for following patients with both prosthetic replacement and implanted tantalum beads: preliminary analysis with a pelvic model and in seven patients. *J Orthop Surg Res* 2016;11(27). <https://doi.org/10.1186/S13018-016-0360-7>
- Balla VK, Bodhak S, Bose S, Bandyopadhyay A. Porous tantalum structures for bone implants: Fabrication, mechanical and in vitro biological properties. *Acta Biomater* 2010;6(8):3349–59. <https://doi.org/10.1016/j.actbio.2010.01.046>
- Jiao J, Hong Q, Zhang D, Wang M, Tang H, Yang J, et al. Influence of porosity on osteogenesis, bone growth and osteointegration in trabecular tantalum scaffolds fabricated by additive manufacturing. *Front Bioeng Biotechnol* 2023;11. <https://doi.org/10.3389/fbioe.2023.1117954>
- Torres AS, Bonitatibus PJ, Colborn RE, Goddard GD, FitzGerald PF, Lee BD, et al. Biological performance of a size-fractionated core-shell tantalum oxide nanoparticle X-ray contrast agent. *Investig Radiol* 2012;47(10):578–87. <https://doi.org/10.1097/RLI.0b013e318260fc40>
- Lambert JW, Sun Y, Stillson C, Li Z, Kumar R, Wang S, et al. An intravascular tantalum oxide-based CT contrast agent: Preclinical evaluation emulating overweight and obese patient size. *Radiology* 2018;289(1):103–10. <https://doi.org/10.1148/radiol.2018172381>
- Freedman JD, Lusic H, Snyder BD, Grinstaff MW. Tantalum oxide nanoparticles for the imaging of articular cartilage using X-ray computed tomography: Visualization of ex vivo/in vivo murine tibia and ex vivo human index finger cartilage. *Angew Chem - Int Ed* 2014;53(32):8406–10. <https://doi.org/10.1002/anie.201404519>
- Hwan Oh M, Lee N, Kim H, Pyo Park S, Piao Y, Lee J, et al. Large-scale synthesis of bioinert tantalum oxide nanoparticles for X-ray computed tomography imaging and bimodal image-guided

- sentinel lymph node mapping. *J Am Chem Soc* 2011;133: 5508–15. <https://doi.org/10.1021/ja200120k>
23. Koshevaya E, Krivoschapkin E, Krivoschapkin P. Tantalum oxide nanoparticles as an advanced platform for cancer diagnostics: a review and perspective. *J Mater Chem B* 2021;9(25):5008–24. <https://doi.org/10.1039/D1TB00570G>
 24. Fitzgerald PF, Butts MD, Roberts JC, Colborn RE, Torres AS, Lee BD, et al. Proposed computed tomography contrast agent using carboxybetaine zwitterionic tantalum oxide nanoparticles imaging, biological, and physicochemical performance. *Investig Radiol* 2016;51(12):786–96. <https://doi.org/10.1097/RLI.0000000000000279>
 25. Chakravarty S, Hix JML, Wiewiora KA, Volk MC, Kenyon E, Shuboni-Mulligan DD, et al. Tantalum oxide nanoparticles as versatile contrast agents for X-ray computed tomography. *Nanoscale* 2020;12(14):7720–34. <https://doi.org/10.1039/D0NR01234C>
 26. Lawson T, Joenathan A, Patwa A, Snyder BD, Grinstaff MW. Tantalum oxide nanoparticles for the quantitative contrast-enhanced computed tomography of ex vivo human cartilage: Assessment of biochemical composition and biomechanics. *ACS Nano* 2021;15(12):19175–84. <https://doi.org/10.1021/acsnano.1c03375>
 27. Fugazzola M, Nissinen MT, Jäntti J, Tuppurainen J, Plomp S, Te Moller N, et al. Composition, architecture and biomechanical properties of articular cartilage in differently loaded areas of the equine stifle. *Equine Vet J* 2023. <https://doi.org/10.1111/evj.13960>
 28. Huttu MRJ, Puhakka J, Mäkelä JTA, Takakubo Y, Tiitu V, Saarakkala S, et al. Cell–tissue interactions in osteoarthritic human hip joint articular cartilage. *Connect Tissue Res* 2014;55(4):282–91. <https://doi.org/10.3109/03008207.2014.912645>
 29. Ebrahimi M, Ojanen S, Mohammadi A, Finnilä MA, Joukainen A, Kröger H, et al. Elastic, viscoelastic and fibril-reinforced poroelastic material properties of healthy and osteoarthritic human tibial cartilage. *Ann Biomed Eng* 2019;47(4):953–66. <https://doi.org/10.1007/s10439-019-02213-4>
 30. Nelson BB, Mäkelä JTA, Patwa AN, Snyder BD, Grinstaff MW, Lawson TB, et al. Cationic contrast-enhanced computed tomography distinguishes between reparative, degenerative, and healthy equine articular cartilage. *J Orthop Res* 2020;39(8): 1647–57. <https://doi.org/10.1002/jor.24894>
 31. Hayes WC, Keer LM, Herrmann G, Mockros LF. A mathematical analysis for indentation tests of articular cartilage. *J Biomech* 1972;5(5):541–51. [https://doi.org/10.1016/0021-9290\(72\)90010-3](https://doi.org/10.1016/0021-9290(72)90010-3)
 32. Ateshian GA, Ellis BJ, Weiss JA. Equivalence between short-time biphasic and incompressible elastic material responses. *J Biomech Eng* 2007;129(3):405–12. <https://doi.org/10.1115/1.2720918>
 33. Mow VC, Kuei SC, Lai WM, Armstrong CG. Biphasic creep and stress relaxation of articular cartilage in compression: Theory and experiments. *J Biomech Eng* 1980;102(1):73–84. <https://doi.org/10.1115/1.3138202>
 34. Shanfield S, Campbell P, Baumgarten M, Bloebaum R, Sarmiento A. Synovial fluid osmolality in osteoarthritis and rheumatoid arthritis. *Clin Orthop Relat Res* 1988;235:289–95 (<http://www.ncbi.nlm.nih.gov/pubmed/3416536>).
 35. Stewart RC, Bansal PN, Entezari V, Lusich H, Nazarian RM, Snyder BD, et al. Contrast-enhanced CT with a high-affinity cationic contrast agent for imaging ex vivo bovine, intact ex vivo rabbit, and in vivo rabbit cartilage. *Radiology* 2013;266(1):141–50. <https://doi.org/10.1148/radiol.12112246>
 36. Mäkelä JTA, Rezaeian ZS, Mikkonen S, Madden R, Han SK, Jurvelin JS, et al. Site-dependent changes in structure and function of lapine articular cartilage 4 weeks after anterior cruciate ligament transection. *Osteoarthr Cartil* 2014;22(6): 869–78. <https://doi.org/10.1016/j.joca.2014.04.010>
 37. Ebrahimi M, Turunen MJ, Finnilä MA, Joukainen A, Kröger H, Saarakkala S, et al. Structure–function relationships of healthy and osteoarthritic human tibial cartilage: Experimental and numerical investigation. *Ann Biomed Eng* 2020;48(12): 2887–900. <https://doi.org/10.1007/s10439-020-02559-0>
 38. Kiviranta I, Jurvelin J, Tammi M, Saamanen AM, Helminen HJ. Microspectrophotometric quantitation of glycosaminoglycans in articular cartilage sections stained with Safranin O. *Histochemistry* 1985;82:249–55.
 39. Király K, Lapveteläinen T, Arokoski J, Törrönen K, Módos L, Kiviranta I, et al. Application of selected cationic dyes for the semiquantitative estimation of glycosaminoglycans in histological sections of articular cartilage by microspectrophotometry. *Histochem J* 1996;28(8):577–90. <https://doi.org/10.1007/BF02331378>
 40. Mankin HJ, Dorfman H, Lippiello L, Zarins A. Biochemical and metabolic abnormalities in articular cartilage from osteoarthritic human hips. II. Correlation of morphology with biochemical and metabolic data. *J Bone Jt Surg* 1971;53(3):523–37.
 41. Mohammadi A, te Moller NCR, Ebrahimi M, Plomp S, Brommer H, van Weeren PR, et al. Site- and zone-dependent changes in proteoglycan content and biomechanical properties of bluntly and sharply grooved equine articular cartilage. *Ann Biomed Eng* 2022;50(12):1787–97. <https://doi.org/10.1007/s10439-022-02991-4>
 42. Rieppo J, Hallikainen J, Jurvelin JS, Kiviranta I, Helminen HJ, Hyttinen MM. Practical considerations in the use of polarized light microscopy in the analysis of the collagen network in articular cartilage. *Microsc Res Technique* 2008;71(4):279–87. <https://doi.org/10.1002/jemt.20551>
 43. Saarakkala S, Julkunen P, Kiviranta P, Mäkitalo J, Jurvelin JS, Korhonen RK. Depth-wise progression of osteoarthritis in human articular cartilage: investigation of composition, structure and biomechanics. *Osteoarthr Cartil* 2010;18(1):73–81. <https://doi.org/10.1016/j.joca.2009.08.003>
 44. Camacho NP, West P, Torzilli PA, Mendelsohn R. FTIR microscopic imaging of collagen and proteoglycan in bovine cartilage. *Biopolym - Biospectrosc Section* 2001;62(1):1–8. [https://doi.org/10.1002/1097-0282\(2001\)62:1<1::AID-BIP10>3.0.CO;2-O](https://doi.org/10.1002/1097-0282(2001)62:1<1::AID-BIP10>3.0.CO;2-O)
 45. Bhattarai A, Mäkelä JTA, Pouran B, Kröger H, Weinans H, Grinstaff MW, et al. Effects of human articular cartilage constituents on simultaneous diffusion of cationic and nonionic contrast agents. *J Orthop Res* 2021;39(4):771–9. <https://doi.org/10.1002/jor.24824>
 46. Honkanen MKM, Matikka H, Honkanen JTJ, Bhattarai A, Grinstaff MW, Joukainen A, et al. Imaging of proteoglycan and water contents in human articular cartilage with full-body CT using dual contrast technique. *J Orthop Res* 2019;37(5):1059–70. <https://doi.org/10.1002/jor.24256>
 47. Paakkari P, Inkien SI, Honkanen MKM, Prakash M, Shaikh R, Nieminen MT, et al. Quantitative dual contrast photon-counting computed tomography for assessment of articular cartilage health. *Sci Rep* 2021;11(1):1–11. <https://doi.org/10.1038/s41598-021-84800-x>
 48. Julkunen P, Kiviranta P, Wilson W, Jurvelin JS, Korhonen RK. Characterization of articular cartilage by combining microscopic analysis with a fibril-reinforced finite-element model. *J Biomech* 2007;40(8):1862–70. <https://doi.org/10.1016/j.jbiomech.2006.07.026>
 49. Boos MA, Grinstaff MW, Lamandé SR, Stok KS. Contrast-enhanced micro-computed tomography for 3D visualization and quantification of glycosaminoglycans in different cartilage types. *Cartilage* 2021;13(2_suppl):486S–94S. <https://doi.org/10.1177/19476035211053820>
 50. Mäkelä JTA, Huttu MRJ, Korhonen RK. Structure-function relationships in osteoarthritic human hip joint articular cartilage.

- Osteoarthr Cartil 2012;20(11):1268–77. <https://doi.org/10.1016/j.joca.2012.07.016>
51. Honkanen JTJ, Turunen MJ, Freedman JD, Saarakkala S, Grinstaff MW, Ylärinne JH, *et al.* Cationic contrast agent diffusion differs between cartilage and meniscus. *Ann Biomed Eng* 2016;44(10):2913–21. <https://doi.org/10.1007/s10439-016-1629-z>
 52. Guilak F, Ratcliffe A, Lane N, Rosenwasser MP, Mow VC. Mechanical and biochemical changes in the superficial zone of articular cartilage in canine experimental osteoarthritis. *J Orthop Res* 1994;12(4):474–84. <https://doi.org/10.1002/JOR.1100120404>
 53. Desrochers J, Amrein MW, Matyas JR. Viscoelasticity of the articular cartilage surface in early osteoarthritis. *Osteoarthr Cartil* 2012;20(5):413–21. <https://doi.org/10.1016/j.joca.2012.01.011>
 54. Hollander AP, Pidoux I, Reiner A, Rorabeck C, Boume R, Poole AR, *et al.* Damage to type II collagen in aging and osteoarthritis starts at the articular surface, originates around chondrocytes, and extends into the cartilage with progressive degeneration. *J Clin Investig* 1995;96(6):2859–69. <https://doi.org/10.1172/JCI118357>
 55. Ebrahimi M, Turkiewicz A, Finnilä MAJ, Saarakkala S, Englund M, Korhonen RK, *et al.* Associations of human femoral condyle cartilage structure and composition with viscoelastic and constituent-specific material properties at different stages of osteoarthritis. *J Biomech* 2022;145, 111390. <https://doi.org/10.1016/j.jbiomech.2022.111390>
 56. Mow VC, Ratcliffe A, Robin Poole A. Cartilage and diarthrodial joints as paradigms for hierarchical materials and structures. *Biomaterials* 1992;13(2):67–97. [https://doi.org/10.1016/0142-9612\(92\)90001-5](https://doi.org/10.1016/0142-9612(92)90001-5)
 57. Miao Z, Liu P, Wang Y, Li K, Huang D, Yang H, *et al.* PEGylated tantalum nanoparticles: A metallic photoacoustic contrast agent for multiwavelength imaging of tumors. *Small* 2019;15(41), e1903596. <https://doi.org/10.1002/SMLL.201903596>
 58. Jin Y, Ma X, Zhang S, Meng H, Xu M, Yang X, *et al.* A tantalum oxide-based core/shell nanoparticle for triple-modality image-guided chemo-thermal synergetic therapy of esophageal carcinoma. *Cancer Lett* 2017;397:61–71. <https://doi.org/10.1016/J.CANLET.2017.03.030>
 59. Saukko AEA, Honkanen JTJ, Xu W, Väänänen SP, Jurvelin JS, Lehto VP, *et al.* Dual contrast CT method enables diagnostics of cartilage injuries and degeneration using a single CT image. *Ann Biomed Eng* 2017;45(12):2857–66. <https://doi.org/10.1007/s10439-017-1916-3>